Electronic Structure of Neutral Tryptophan Radicals in Ribonucleotide Reductase Studied by EPR and ENDOR Spectroscopy

Friedhelm Lendzian,*,† Margareta Sahlin,§ Fraser MacMillan,†,⊥ Robert Bittl,† Robert Fiege,† Stephan Pötsch,‡ Britt-Marie Sjöberg,§ Astrid Gräslund,‡ Wolfgang Lubitz,† and Günter Lassmann*,†,#

Contribution from the Max-Volmer-Institut für Biophysikalische Chemie und Biochemie, Technische Universität Berlin, D-10623-Berlin, Germany, Department of Molecular Biology and Department of Biophysics, University of Stockholm, S-10691, Stockholm, Sweden, and Max-Delbrück-Centrum für Molekulare Medizin, D-13125-Berlin, Germany

Received March 20, 1996[⊗]

Abstract: Two different tryptophan radicals ($W_a^\bullet$ and $W_b^\bullet$) with lifetimes of several minutes at room temperature are formed during the reconstitution of the diiron center in the *Escherichia coli* ribonucleotide reductase mutant protein R2 Y122F. Detailed hyperfine parameters are for the first time determined for protein-linked oxidized neutral tryptophan radicals. $W_a^\bullet$ is freeze-trapped and investigated by EPR and ENDOR in protonated and selectively deuterated proteins at 20 K. Two hyperfine couplings from the β-methylene protons, hyperfine tensors of two α-protons, and the complete nitrogen hyperfine tensor are determined. Based on the absence of a large hyperfine coupling from the N−H proton, which would be expected for a cation radical, and on comparison of the experimental data with theoretical spin densities from density functional calculations, $W_a^\bullet$ is assigned to an oxidized neutral tryptophan radical. A small anisotropic hyperfine coupling detected in selectively deuterated $W_a^\bullet$ is tentatively assigned to a proton which is hydrogen bonded to the nitrogen of $W_a^\bullet$. A similar spin density distribution as for $W_a^\bullet$ is obtained also for the second tryptophan radical, $W_b^\bullet$, observed by EPR at room temperature, which is also assigned to an oxidized neutral radical.

1. Introduction

Ribonucleotide reductase catalyses the reduction of ribonucleotides to deoxyribonucleotides and is therefore a key enzyme for cell proliferation. Recent reviews about the structure and function of this enzyme are given in refs 1 and 2. Class I ribonucleotide reductases consist of two proteins R1 and R2, both of which are homodimers. R1 contains the binding sites for substrates and allosteric effectors, and R2 carries the dinuclear iron site and the tyrosyl radical $Y122^\bullet$. Both proteins are necessary for the enzymatic activity. The three-dimensional structures of R1[3] and R2[4] from *Escherichia coli* have been determined by X-ray diffraction. In active protein R2 the two high-spin ferric ions are antiferromagnetically coupled via a μ-oxo-bridge.[5,6] $Y122^\bullet$ is an oxidized neutral radical.[7,8] From ENDOR investigations it was concluded that no hydrogen bond is formed between $Y122^\bullet$ and surrounding protein residues.[9] The diiron site of R2 and its amino acid environment is depicted in Figure 1.

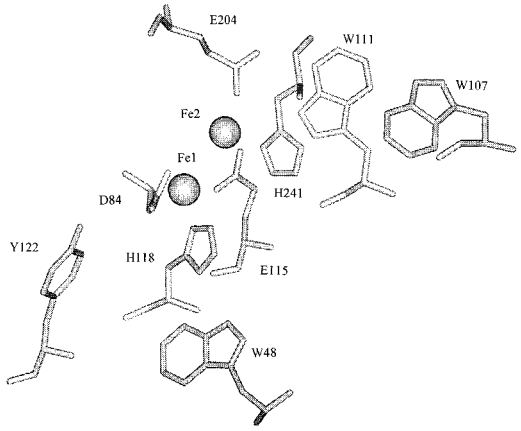

Figure 1. X-ray structure of the diiron site including neighboring amino acid residues of *E. coli* ribonucleotide reductase protein R2 [4]. (For clarity the Fe2 ligand E238 has been excluded.)

Using the X-ray structure of the two proteins a model of the active holoenzyme has been built.[1,3] In this model the tyrosyl radical in R2 is situated about 35 Å away from the substrate binding site in protein R1. A series of amino acids, conserved in ribonucleotide reductases of several organisms,[1] forms a network of hydrogen bonds which has been proposed as an electron transfer pathway between the substrate binding site in

* To whom correspondence should be addressed: Fax (+49 30) 31 42 11 22.
† Max-Volmer-Institut für Biophysikalische Chemie und Biochemie.
§ Department of Molecular Biology, University of Stockholm.
‡ Department of Biophysics, University of Stockholm.
# Max-Delbrück-Centrum für Molekulare Medizin.
⊥ Present address: Section de Bioenergetique, DBCM, C.E. Saclay, 91191, Gif-sur-Yvette, France.
⊗ Abstract published in *Advance ACS Abstracts,* August 1, 1996.

(1) Sjöberg, B.-M. In *Nucleic Acids and Molecular Biology*; Vol. 9, Eckstein, F., Lilley, D. M. J., Eds.; Springer: Berlin, 1995; Vol. 9, pp 192−221.
(2) Stubbe, J.; van der Donk, W. *Chem. Biol.* **1995**, *2*, 793−801.
(3) Uhlin, U.; Eklund, H. *Nature* **1994**, *370*, 533−539.
(4) (a) Nordlund, P.; Sjöberg, B.-M.; Eklund, H. *Nature* **1990**, *345*, 593−598. (b) Nordlund, P.; Eklund, H. *J. Mol. Biol.* **1993**, *232*, 123−164.
(5) Petersson, L.; Gräslund, A.; Ehrenberg, A.; Sjöberg, B.-M.; Reichard, P. *J. Biol. Chem.* **1980**, *255*, 6706−6712.
(6) (a) Sjöberg, B.-M.; Loehr, T. M.; Sanders-Loehr, J. *Biochemistry* **1982,** *21*, 96−102. (b) Ling, J.; Sahlin, M.; Sjöberg, B.-M.; Loehr, T. M.; Sanders-Loehr, J. *J. Biol. Chem.* **1994**, *269*, 5595−5601.
(7) Gräslund, A.; Sahlin, M. *Annu. Rev. Biophys. Biomol. Struct.*, In press.
(8) Backes, G.; Sahlin, M.; Sjöberg, B.-M.; Loehr, T. M.; Sanders-Loehr, J. *Biochemistry* **1987**, *28*, 1923−1926.
(9) Bender, C. J.; Sahlin, M.; Babcock, G. T.; Barry, B. A.; Chandrashekar, T. K.; Salowe, S. P.; Stubbe, J.; Lindström, B.; Peterson, L.; Ehrenberg, A.; Sjöberg, B.-M. *J. Am. Chem. Soc.* **1989**, *111*, 8076−8083.

S0002-7863(96)00917-1 CCC: $12.00

R1 and Y122• in R2.[10] In R2, this network involves D84, Fe1, H118, D237, and W48. A similar hydrogen-bonded triad of amino acids is also found in cytochrome *c* peroxidase, where the tryptophan cation radical W191• is connected via D235 and H175 with the heme iron.[11−13]

Removal of the dinuclear iron center from R2 is accompanied by a loss of the radical at Y122 leading to the inactive apoprotein R2. The catalytically essential iron/radical center can, however, be reconstituted in a reaction with ferrous iron and molecular oxygen according to the general scheme[5,14]

$$\underset{\text{(apoR2)}}{\text{P/TyrOH} + 2\text{Fe}^{2+} + \text{O}_2 + \text{H}^+ + \text{e}^-} \rightarrow \underset{\text{(active R2)}}{\text{P/Fe}^{\text{III}}\text{−O}^{2-}\text{−Fe}^{\text{III}}\text{/TyrO}^\bullet + \text{H}_2\text{O}} \quad (1)$$

where P denotes the polypeptide chain and TyrOH indicates Y122 in wild-type R2 protein. The formation of the dinuclear iron center is a multistep reaction where a number of intermediate radicals and redox states of the diiron center have previously been observed.[15−18]

In the mutant R2 Y122F, the protein is deprived of one reducing equivalent that is normally provided by Y122 in the wild-type protein. The F122 residue is not oxidized, but instead other free radicals are formed during the reconstitution reaction. Two of the six different paramagnetic species formed upon reconstitution of R2 Y122F have been identified as tryptophan free radicals using selective deuterium labeling.[17,18] These two radicals exhibit different kinetics of formation, different hyperfine splitting patterns, and different EPR saturation behavior. Both radicals have lifetimes on the minute time scale at room temperature. One tryptophan radical is best observed at $T \leq 77$ K due to relatively fast spin relaxation[18] and is hereafter called $W_a^\bullet$, and the tryptophan radical which is observed at room temperature[18] is denoted $W_b^\bullet$.

This study focuses on a detailed characterization of the oxidation state and the electronic structure of these two tryptophan radicals. EPR and ENDOR spectroscopy at 20 K are used in combination with simulations of EPR powder spectra to determine the hyperfine (hf) tensors of the nitrogen atom, both β-methylene protons, two of the α-protons and one proton probably hydrogen bonded to nitrogen N1 of the $W_a^\bullet$ radical (for protons the standard EPR terminology α, β, and γ is used, which refers to the nearest atom in the conjugated π-system,[9] see Figure 2). Spin densities derived from the experimental data are compared with results obtained from advanced molecular orbital and density functional theory (DFT) calculations. The results represent the first detailed characterization of protein-linked oxidized neutral tryptophan radicals.

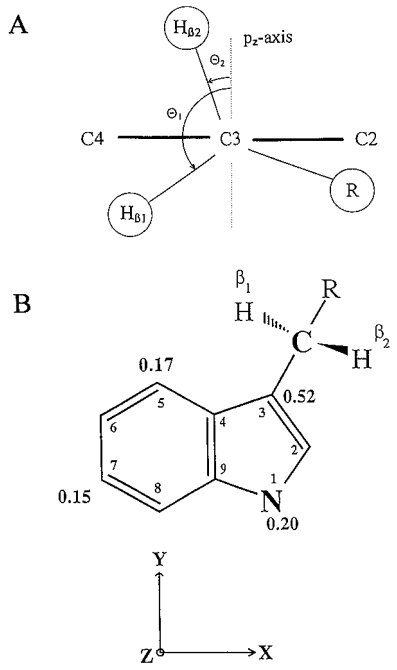

Figure 2. (A) Conformation of β-methylene-protons $H_{\beta 1}$ and $H_{\beta 2}$ and corresponding dihedral angles Θ of tryptophan W111 ($\Theta_1 = -133°$, $\Theta_2 = -10°$) in protein R2 [4]. Positive Θ's are counted clockwise from the p_z axis. (B) Molecular structure, numbering scheme (inner numbers), and axes systems of the tryptophan neutral radical, deprotonated at the indole nitrogen. The bold numbers are the experimentally determined π-spin densities for the respective carbon and nitrogen positions. (See Table 2).

2. Material and Methods

2.1. Protein Preparation. Overproduction of mutant protein R2 Y122F was achieved in *E. coli* strain MC1009 containing plasmids pGP1−2 and MK5, the latter being a recombinant derivative of pTZ18R containing the mutant nrdB gene.[19] ApoR2 Y122F was obtained by growing this strain in an iron-depleted medium (with or without tryptophan-d_5).[20] The protein was purified as described earlier.[21,22] L-Tryptophan-d_5 (98%) (deuterated at positions 2, 5, 6, 7, and 8; see Figure 2) was obtained from Cambridge Isotope Laboratories Ltd.

2.2. Generation of Tryptophan Radicals in Protein R2 Y122F. The overall activation reaction of wild-type apoR2 follows reaction 1. The mutant samples for low temperature EPR and ENDOR studies were prepared by mixing of the apoR2 Y122F (1.8 mM in 50 mM Tris−HCl buffer, pH 7.6, saturated with oxygen gas) with an equal volume of an anaerobic solution of ferrous ammonium sulfate (7.2 mM in Tris−HCl buffer, pH 7.6) in a 3 mm i.d. EPR quartz tube. After 26 s reaction time at room temperature the samples were frozen using cold isopentane (170 K) and stored at 77 K.

For room temperature EPR studies using a stopped-flow EPR accessory (see below) aerobic apoR2 Y122F (100 μM) was mixed (1:1) with anaerobic ferrous ammonium sulfate (400 μM).

2.3. EPR and ENDOR Instrumentation. X-band EPR spectra were measured with a Bruker ESP-300E spectrometer using the standard rectangular Bruker EPR cavity (ER4102T) and an Oxford helium flow cryostat (ESR 9) for temperature control. ENDOR spectra were recorded with a Bruker ESP-300E spectrometer, using a self-built ENDOR extension consisting of a Rhode & Schwarz RF synthesiser (SMT02), an ENI solid state RF amplifier (A200L), and a laboratory built high-Q TM_{110} ENDOR cavity[23] adapted to an Oxford helium flow

(10) Sjöberg, B.-M. *Structure* **1994**, *2*, 793−796.
(11) Houseman, A. L. P.; Doan, P. E.; Goodin, D. B.; Hoffman, B. M. *Biochemistry* **1993**, *32*, 4430−4443.
(12) Sivaraja, M.; Goodin, D. B.; Smith, M.; Hoffman, B. M. *Science* **1989**, *245*, 738−740.
(13) Huyett, J. E.; Doan, P. E.; Gurbiel, R.; Houseman, A. L. P.; Sivaraja, M.; Goodin, D. B.; Hoffman, B. M. *J. Am. Chem. Soc*. **1995**, *117*, 9033−9041.
(14) Ochiai, E. I.; Mann, G.; Gräslund, A.; Thelander, L. *J. Biol. Chem.* **1990,** *265*, 15758−15761.
(15) Bollinger, J. M.; Tong, W. H.; Ravi, N.; Huynh, B. H.; Edmondson, D. E.; Stubbe, J. *J. Am. Chem. Soc*. **1994**, *116*, 8015−8023.
(16) Bollinger, J. M.;Tong, W. H.; Ravi, N.; Huynh, B. H.; Edmondson, D. E.; Stubbe, J. *J. Am. Chem. Soc*. **1994,** *116*, 8024−8032.
(17) Sahlin, M.; Lassmann, G.; Pötsch, S.; Slaby, A.; Sjöberg, B.-M.; Gräslund, A. *J. Biol. Chem*. **1994**, *269*, 11699−11702.
(18) Sahlin, M.; Lassmann, G.; Pötsch, S.; Sjöberg, B.-M.; Gräslund, A. *J. Biol. Chem.* **1995**, *270*, 12361−12372.
(19) Larsson, Å.; Sjöberg, B.-M. *EMBO J.* **1986**, *5*, 2037−2040.
(20) Åberg, A.; Ormö, M.; Nordlund, P.; Sjöberg, B.-M. *Biochemistry* **1993**, *32*, 9845−9850.
(21) Sjöberg, B.-M.; Hahne, S.; Karlsson, M.; Jörnvall, H.; Göransson, M.; Uhlin, B. E. *J. Biol. Chem*. **1986**, *261*, 6558−5662.
(22) Sjöberg, B.-M.; Karlsson, M.; Jörnvall, H. *J. Biol. Chem*. **1987**, *262*, 9736−9743.
(23) Zweygart, W.; Thanner, R.; Lubitz, W. *J. Magn. Reson*. **1994** *109*, 172−177.

cryostat (ESR 910). Spin concentrations were determined by comparison of double integrals of EPR spectra with that of the tyrosyl radical Y122• in a wild-type R2 sample which had been calibrated with a frozen standard Cu^{2+} solution.

Room temperature EPR spectra were recorded with a Bruker EPR spectrometer ESP 300E (H_{102} cavity) and a stopped-flow EPR accessory specially designed at the Max-Delbrück-Center (Berlin) for biological application (70 μL of each reagent/shot).[24] After each flow-stop cycle several rapid field scans were accumulated in the time window between 1 and 12 min.

2.4. EPR Powder-Spectra Simulation. The EPR powder spectra have been analyzed using a program for simulation and fitting of EPR spectra with anisotropic **g** and hf tensors based on the work of Rieger.[25] The spectra were simulated by computing the resonant field position at the given microwave frequency dependent on the orientation of the tensors with respect to the external magnetic field. The superposition of all orientations for the randomly oriented powder-like sample was performed employing a spiral approach,[26] typically using 1000 grid points.

This approach[25] yields the resonant field position, correct to second order, for the Hamiltonian

$$\mathrm{H} = \mu_{\mathrm{B}} S\mathbf{g}B + \sum_i S\mathbf{A}_i I_i \qquad (2)$$

where **g** and S are the electronic **g** tensor and spin operator; $\mathbf{A_i}$ and I_i are the hf tensor and spin operator of the ith nucleus, B is the magnetic field vector, and μ_B is the Bohr magneton. No restrictions for the relative orientation of the principal axes of the different tensors exist. The principal axis system of **g** serves as a reference system and the orientations of the hf tensors, $\mathbf{A}_i$, are given by the Euler angles, $\Omega_i = (\alpha_i,\beta_i,\gamma_i)$. The resulting histogram of resonant field positions is folded with a combined Lorentzian and Gaussian line shape function, finally yielding the derivative EPR spectrum. A nonlinear least-squares routine is used to find the optimum set of parameters for best simulating a given experimental spectrum.

2.5. Calculation of Spin Densities. 2.5.1. Molecular Orbital (MO) Calculations (RHF-INDO/SP). MO calculations for tryptophan radicals were performed using the RHF-INDO/SP (restricted Hartree−Fock, intermediate neglect of differential overlap, spin polarization) method.[27] This method uses the INDO parametrization of Pople[28] and a restricted Hartree−Fock formulation. Spin polarization effects due to interaction of the unpaired electron with paired electrons of other orbitals are treated as perturbations.[27] Coordinates of tryptophans W48, W107, and W111 in R2 protein (chain A) were taken from the X-ray data.[4] Protons were attached to the appropriate heavy atom coordinates using standard software ("Insight II", Molecular Simulations). The calculations yielded atomic p-(π-)spin densities as well as s-spin densities, and theoretical isotropic hyperfine couplings constants were obtained from the s-spin densities using the geometry-independent Q factors, 1420 MHz for ^{1}H and 650 MHz for ^{14}N.[27]

2.5.2. Density Functional Theory (DFT) Calculations. Recently, density functional theory (DFT) methods have become available for *ab initio* calculations of spin densities of moderate size molecules with the Gaussian 92/DFT program[29] or the DMol program.[30] Gaussian92/DFT has been used by Jensen et al.[31] to study the effect of different basis sets, available in this program, on calculated geometries, energies, and spin densities of the neutral and cation radical of 3-methylindole. These DFT results have been compared with Møller−Plesset (MP) perturbation theory *ab initio* calculations.[31] The DFT spin densities were found to agree better with experimental data for the tryptophan-191 radical in cytochrom *c* peroxidase[13] than the MP results. Here we used the DMol program to give independent DFT results for spin densities of the 3-methylindole radicals. For all calculations we used the nonlocal spin density approximation BPW functional, i.e. the DMol implementation of the Perdew and Wang generalized gradient approximation for the correlation functional[32] and the Becke gradient corrected exchange functional.[33] We employed the DNP basis, a double-numerical basis set including polarization functions. The use of a numerical atomic orbital basis set in our DMol calculations is an important difference compared to the use of Gaussian orbital basis sets in Gaussian 92/DFT calculations of refs 31 and 34. In a first step a geometry optimization was performed for both radicals (neutral and cation) using frozen core orbitals. Thereafter a second geometry optimization with all electrons included in the self-consistent field (SCF) cycles was performed. For the resulting optimized geometries of the oxidized tryptophan neutral and cation radical Mulliken spin densities were calculated.

3. Results

3.1. EPR and ENDOR Spectra of the Tryptophan Radical W_a• at Low Temperature. EPR spectra consisting of two components have been observed at 77 K after reaction of aerobic apoR2 Y122F at room temperature with anaerobic Fe^{2+} between 6 s and 10 min.[18] The two species could be distinguished by their different EPR saturation behavior and their different lifetimes at room temperature. One species that was easier to saturate exhibited a large **g**-tensor anisotropy ($g_{\|} = 2.036$ and $g_{\perp} = 2.009$) and no resolved hyperfine structure and will not be further considered in the present study. At high protein concentrations this species is apparently suppressed (data not shown). The second species which is the main component at high protein concentrations shows a resolved hyperfine splitting dominated by a four-line pattern. This second species, denoted W_a• in this study (component II in ref 18), was previously assigned to a tryptophan radical using R2 Y122F containing selectively deuterated tryptophans.[18]

3.1.1. EPR. Figure 3A shows the EPR spectrum of W_a• (ca. 60 μM) in highly concentrated protein R2 Y122F (0.9 mM) at 20 K. The dominating four-line pattern previously observed at 77 K[17,18] shows at 20 K a resolved hyperfine structure of each component. In order to identify the hfc's resulting from protons attached to the ring system (positions 2 and 5 to 8, see Figure 2) we have also studied this radical in R2 Y122F with tryptophan-d_5 in H_2O buffer. In the EPR spectrum of W_a• of the selectively deuterated sample obtained at 20 K (Figure 3B) the small hyperfine splittings of the four central lines have disappeared, and well-resolved shoulders appear at the outer wings of the spectrum. Line-shape analysis indicates that the four intense central lines result from nearly isotropic hfc's, whereas the shoulders are turning points of a pronounced anisotropic hyperfine powder pattern, which results from a large anisotropic ^{14}N coupling. In this case only the m_I (^{14}N) = ±1 components in the EPR spectrum are additionally broadened by the anisotropic ^{14}N hf interaction, whereas the $m_I(^{14}\mathrm{N}) = 0$ components are not affected. For a large spin density in the nitrogen p_z orbital the purely dipolar ^{14}N-hyperfine (hf) tensor $\mathbf{A}'$ is axially symmetric with principal values $A'_{zz} = 2B$ along the z axis of the p_z orbital and $A'_{xx} = A'_{yy} = -B$ along the x

(24) Lassmann, G.; Thelander, L.; Gräslund, A. *Biochem. Biophys. Res. Commun.* **1992**, *188*, 879−887.
(25) Rieger, P. H. *J. Magn. Reson.* **1982**, *50*, 485−489.
(26) Mombourquette, H. J.; Weil, J. E. *J. Magn. Reson.* **1992**, *99*, 37−44.
(27) (a) Plato, M.; Möbius, K.; Lubitz, W. In *Chlorophylls* ; Scheer, H., Ed.; CRC Press, Boca Raton, 1990; pp. 1015−1046. (b) Plato, M.; Lendzian, F.; Lubitz, W.; Möbius, K. In *The Photosynthetic Bacterial Reaction Center II, Structure, Spectroscopy and Dynamics;* Breton, J., Vermeglio, A., Eds.; Plenum Press: New York, 1992; pp 109−118.
(28) Pople, J. A.; Beveridge, D. L. *Approximate Molecular Orbital Theory;* McGraw-Hill Inc.: New York, 1970.
(29) Frisch, M. W. et al. GAUSSIAN92/DFT; GAUSSIAN94 (Revision B.1); Gaussian, Inc.: Pittsburgh, PA, 1995.
(30) DMol Release 95.0, Molecular Simulations Inc.: San Diego, CA, 1995.
(31) Jensen, G. M.; Goodin, D. B.; Bunte, S. W. *J. Phys. Chem.* **1996**, *100*, 654−959.
(32) Perdew, J. P.; Wang, Y. *Phys. Rev.* **1992**, *B45*, 13244.
(33) Becke, A. D. *J. Chem. Phys.* **1988**, *88*, 2547.
(34) Walden, S. E.; Wheeler, R. A. *J. Phys. Chem.* **1996**, *100*, 1530−1535.

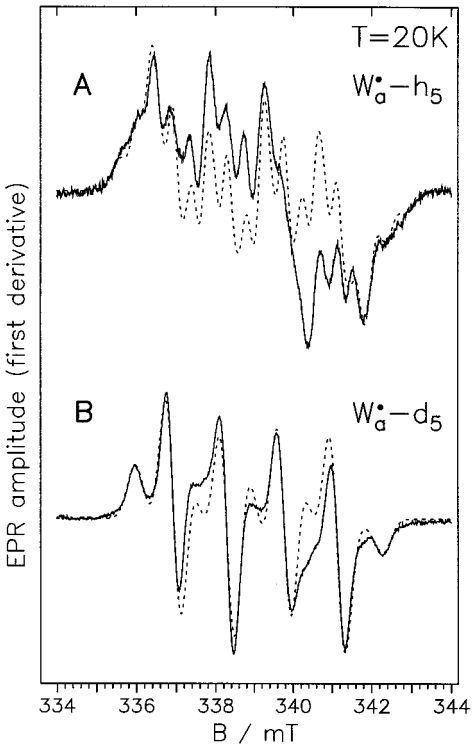

Figure 3. EPR spectra at 20 K of the tryptophan radical $W_a^\bullet$ observed after reconstitution of *E. coli* apoprotein R2 Y122F (0.9 mM) with ferrous iron (3.6 mM) and oxygen, freeze-quenched after a reaction time of 26 s at 25 °C. (A) R2 with protonated tryptophan. (B) R2 with tryptophan-d_5. Solid lines: experiment, dotted lines: best simulation (fit). Experimental conditions: microwave power, 0.1 mW; field modulation, 12.5 kHz; amplitude, ± 0.1 mT peak to peak. For the fits and simulations a Gaussian line width of 0.26 and 0.36 mT was used for A and B, respectively, the obtained **g** and hf tensors are given in Table 1. Remaining deviations of the amplitudes of experimental and simulated spectra are attributed to a second minor species (probably due to a small amount of $W_b^\bullet$).

and *y* axes. The isotropic part is positive and of similar magnitude as *B*. The resulting complete tensor including the isotropic term has principal values $A_{zz} \approx 3B$ and $A_{xx} \approx A_{yy} \approx 0$.[35] The spectral A_{xx} and A_{yy} components of the $m_I(^{14}N) = \pm 1$ EPR transitions are hence superimposed on the narrow line resulting from the $m_I(^{14}N) = 0$ component. Such a spectral shape is typically observed also for nitroxide radicals.[36] This pattern holds for each of the four prominent lines in Figure 3B. The anisotropic shoulders of the $m_I(^{14}N) = \pm 1$ transitions are, however, clearly resolved only for the outer lines due to the spectral overlap in the center of the EPR spectrum.

The hyperfine couplings leading to the prominent four-line structure of the EPR spectrum (Figure 3B) have no observable anisotropy. A small anisotropy is typical for hfc's of β-protons; four lines with equal line intensities are obtained from the two β-protons (Figure 2) when the ratio of the two hfc's (β_1 and β_2) is 2:1. The fit of the EPR spectrum (Figure 3B, dashed line) based on two isotropic proton-hfc's (1.36 and 2.83 mT) and one large anisotropic ^{14}N-hf tensor (see Table 1) is in good agreement with the experimental EPR spectrum. This holds in particular for the peak positions and the zero crossings. The hyperfine and **g** tensor principal values obtained from the fit of Figure 3B are given in Table 1.

The **g**-tensor principal values, which are all close to the free electron value (2.0023), and the small *g* anisotropy is typical for an organic π-radical with large spin densities only on carbon or nitrogen atoms. Radicals with large spin densities on heavier atoms (e.g. oxygen), like the tyrosyl radical $Y122^\bullet$ of R2 or semiquinone anion radicals, exhibit significantly larger g_{xx} and g_{yy} values, also leading to increased isotropic *g* values.[37,38] The principal axis corresponding to the smallest **g**-tensor principal value (g_{zz} in $W_a^\bullet$) is assumed to be parallel to the normal of the molecular plane as usually found for organic π-systems.[39]

The large ^{14}N hyperfine tensor component $A_{zz} = 1.05$ mT indicates significant π-spin density at the nitrogen nucleus. The EPR simulations (Figure 3B) provide an upper limit of about 0.1 mT for A_{xx} and A_{yy} (see Table 1). Any proton hyperfine coupling additional to those of the two β-protons, which is not resolved in Figure 3B, but may contribute to the EPR line width (e.g. from a possible N−H proton which is exchangeable, see below), has to be less than 0.2 mT according to the simulations.

The EPR spectrum of fully protonated $W_a^\bullet$ (Figure 3A) shows additional splittings due to ring α-protons (position 2 and positions 5 to 8). For the simulations and fits of the EPR spectrum of protonated $W_a^\bullet$ the parameters obtained from $W_a^\bullet$-d_5 (*g* and ^{14}N-hf tensors, and hfc's of the β-protons β_1 and β_2) were kept constant. Part of the α-proton hf-tensor elements were derived from ENDOR. The obtained hf tensor principal values and assignments are given in Table 1 and are discussed below.

3.1.2. ENDOR. ENDOR experiments were performed on protein R2 Y122F with either protonated tryptophan (Figure 4A) or tryptophan-d_5 (Figure 4B). The ENDOR resonance condition is given by

$$\nu_\pm(\text{ENDOR}) = |\nu_n \pm A/2| \qquad (3)$$

where $\nu_\pm$ are the high- and low-frequency shifted ENDOR transitions, ν_n is the respective nuclear Zeeman frequency (14.4 MHz for a proton, 2.2 MHz for a deuteron, and 1.04 MHz for ^{14}N for a magnetic field of 339 mT), and *A* is the hyperfine coupling constant. For each hyperfine coupling *A* two ENDOR lines are expected which are spaced symmetrically around ν_n and separated by *A* in the case of $|A/2| < \nu_n$. For $|A/2| > \nu_n$ the lines are spaced around $|A/2|$ and separated by $2\nu_n$. In frozen disordered solution, peaks are observed in the first derivative ENDOR spectra for each principal value A_{ii} ($i = 1, 2, 3$) of a hyperfine (hf) tensor. The ENDOR spectra of $W_a^\bullet$ are dominated by strong matrix lines at the proton Larmor frequency, which result from weakly coupled protons of the surrounding and some small hyperfine shifted lines at the wings of the strong matrix line.

***β*-Protons:** The ENDOR lines of the two β-protons are expected at 4.5, 33.5, 25.5, and 54.5 MHz. Due to the large magnitude of the hfc of these β-protons (38 and 79 MHz), the expected ENDOR line widths must be of the order of several megahertz even though the hyperfine anisotropy of β-protons is only about 10% of the isotropic value. This probably reduces the signal intensity beyond detection, and therefore no ENDOR lines were detected at these frequencies. It should be noted in this context that the yield of $W_a^\bullet$ radicals in R2 Y122F is more than one order of magnitude smaller than that of $Y122^\bullet$ radicals in the wild-type R2 of *E. coli* studied previously by ENDOR.[9]

(35) Carrington, A.; McLachlan, A. D. *Introduction to Magnetic Resonance*, Harper & Row, New York, 1969.

(36) Berliner, L. J.; Reuben, J. Biological Magnetic Resonance. *Spin Labeling, Theory and Application;* Plenum Press: New York, 1989; Vol. 8.

(37) Gerfen, G. J.; Bellew, B. F.; Un, S.; Bollinger, J. M.; Stubbe, J.; Griffin, R.G.; Singel, D. J. *J. Am. Chem. Soc.* **1993**, *115*, 6420−6421.

(38) Burghaus, O.; Plato, M.; Roher, R.; Möbius, K.; MacMillan, F.; Lubitz, W. *J. Phys. Chem.* **1993**, *97*, 7639−7647.

(39) Atherton V. M. *Electron Spin Resonance—Theory and Application*; John Wiley & Sons Inc.: New York, 1973; Chapter 3.12.

Table 1. Experimental Electronic **g** Tensor (g_{ii}) and Hyperfine Tensor (A_{ii} [mT]) Principal Values of $W_a^\bullet$ and $W_b^\bullet$ in Protein R2 Y122F of *E. coli* Ribonucleotide Reductase

radical	tensor element	g_{ii} [b]	$A_{ii}(^{14}N)$	$A_{ii}(\beta_1)$[c]	$A_{ii}(\beta_2)$[c]	A_{ii}(H5)[d]	A_{ii}(H7)[d]	A_{ii}(HB)[e]
$W_a^\bullet$ [a]	*xx*	2.0031(1)	≤|0.10|	1.36(2)	2.83(2)	−0.63(2)	≤|0.15|	−0.118(5)
(20 K)	*yy*	2.0031(1)	≤|0.10|	1.36(2)	2.83(2)	≤|0.15|	−0.56(2)	0.193(5)
	zz	2.0023(1)	1.05(2)	1.36(2)	2.83(2)	−0.52(2)	−0.46(2)	−0.079(5)
	iso	2.0028(1)	0.40	1.36	2.83	−0.40	−0.36	
$W_b^\bullet$ [f]	*xx*	2.0031(2)	0.22(4)	≤0.2	1.60(4)	−0.70(10)	−0.35(10)	
(293 K)	*yy*	2.0031(2)	0.22(4)	≤0.2	1.60(4)	−0.40(10)	−0.60(10)	
	zz	2.0028(2)	0.87(4)	≤0.2	1.60(4)	−0.65(10)	−0.38(10)	
	iso	2.0030(2)	0.44	≤0.2	1.60	−0.58	−0.44	

[a] From fits of the EPR powder spectra (Figure 3) and from ENDOR data (Figure 4) of protonated tryptophan and tryptophan-d_5. Values in brackets are estimated errors in the last digit. [b] Values for $W_a^\bullet$ were calibrated against a DPPH sample which has been calibrated against a Li/LiF standard ($g = 2.00228(2)$).[53] The isotropic g factors g_{iso} of $W_a^\bullet$ and $W_b^\bullet$ agree within their errors. [c] Different hfc's for β_1 and β_2 of $W_a^\bullet$ and $W_b^\bullet$ are discussed in the text. [d] The axes corresponding to the largest principal values of the hyperfine-tensors of H5(*xx*) and H7(*yy*) are in the molecular $x-y$ plane (see Figure 2) and make an angle of approximately 90° according to the EPR simulations. For assignment to positions 5 and 7 see text. Calculated direction cosines are given in Table 3. [e] Principal values of the hyperfine tensor assigned to a proton hydrogen bonded to N1 (from ENDOR, Figure 4B, see also text). Signs from calculated tensors (Table 3). According to the calculated direction cosines the principal axis of the largest positive value builds an angle of 12° with the molecular *y*-axis and lies in the molecular plane. From the spin density distribution given in Table 2 and Figure 2 a N···H distance of ca. 1.75 Å is calculated (see Table 3). [f] All tensors (g and hyperfine) of $W_b^\bullet$ show a reduced anisotropy which is tentatively attributed to the slow rotational motion of the protein (see text). The different hfc's β_1 and β_2 as compared with $W_a^\bullet$ are discussed in the text.

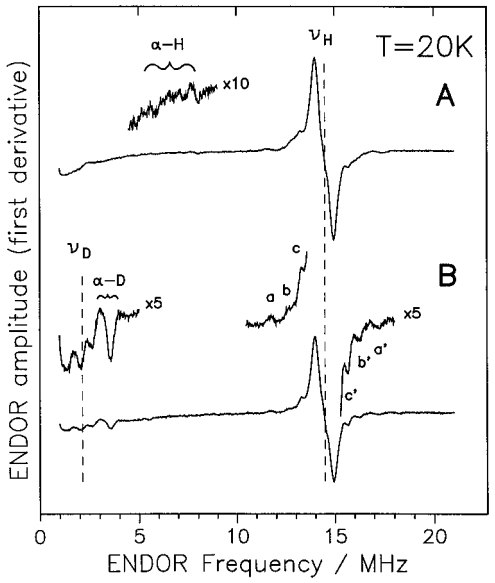

Figure 4. ENDOR spectra at 20 K of the tryptophan radical $W_a^\bullet$ observed after reconstitution of *E. coli* apoprotein R2 Y122F (0.9 mM) with ferrous iron (3.6 mM) and oxygen, freeze-quenched after a reaction time of 26 s at 25 °C. (A) R2 with protonated tryptophan. (B) R2 with tryptophan-d_5. Inserts show the spectral range of the low-frequency α-proton lines (A) and α-deuteron and H-bond proton lines (B) with enlarged amplitudes. Spectra were recorded with the field setting on the second line (starting from low field) of the four major EPR lines in order to avoid contributions from a weak additional EPR signal superimposed on the third line (see Figure 3). Background traces obtained with an EPR setting 10 mT off-resonance were subtracted. Experimental conditions: microwave power, 5 mW; Rf power, 100−150 W; fm, modulation frequency, 1.56 kHz; amplitude, ±100 kHz. Total accumulation time (A) 1 h and (B) 30 min.

The large hfc's of these β-protons were, however, obtained here with high accuracy from fits of the EPR powder spectra (see Table 1).

^{14}N: The turning points of the ^{14}N powder ENDOR spectrum can be calculated from the hf tensor principal values obtained from the EPR simulations. According to eq 3 two peaks are expected for each principal value, which are separated by $2\nu_n$ (i.e. $\nu_\pm = |(A_{ii}/2) \pm \nu_n|$, $i = x, y, z$; for axial symmetry $A_{zz} = A_{||}$ and $A_{xx} = A_{yy} = A_\perp$). The calculated $A_{||}$ peaks ($A_{zz} = 1.05$ mT) are at 14.7 ± 1 MHz, those for $A_\perp$ ($A_{xx} = A_{yy} \leq 0.1$ mT) are at 1.4 ± 1 MHz. Since the intensity of the ^{14}N-ENDOR transitions is spread over the whole spectral range between 0.4 and 15.7 MHz only weak signal amplitudes can be expected. In addition, quadrupolar splittings in the order of several megahertz are expected, which in frozen solution give rise to additional broadening. The ENDOR peaks corresponding to $A_{||}$ are expected in the region of the broad and strong proton matrix ENDOR line (Figure 4A) and are therefore hard to detect. There is a feature at about 2.5 MHz in Figure 4A which could be assigned to the high-frequency $A_\perp$ component ($\nu_+ = A_\perp/2 + \nu_n$). For this assignment $A_\perp = A_{xx} = A_{yy} = 0.1$ mT is obtained, which is consistent with the result from the EPR simulation (≤0.1 mT, see Table 1).

α-Protons: The ENDOR signals of the α-positions directly attached to the indole ring are best observed in the deuterium ENDOR spectrum of $W_a^\bullet$-d_5 (Figure 4B). Due to the smaller magnetic moment of deuterons all hyperfine splittings are reduced with respect to protons by a factor $\gamma_H/\gamma_D = 6.5$ where γ_H and γ_D are the gyromagnetic ratios of the proton and deuteron, respectively. This results in an ENDOR spectrum shifted and compressed by the same factor which leads to increased signal intensities in case of large hyperfine anisotropy. Three deuterium ENDOR signals are distinguished in the frequency range of 1.5 to 4 MHz (Figure 4B).

Typical hf-tensor principal values of an α-proton (C−H fragment) are 90, 60, and 30 MHz for a π-spin density of 1.0 at the adjacent carbon atom.[35] The expected ENDOR positions for a deuteron have to be scaled by the smaller magnetic moment of deuterons and by the actual carbon π-spin density. We assign the line near 2.5 MHz to the smallest hf tensor principal value and the broader line between 3.0 and 3.5 MHz to the two larger principal values of a deuteron in the α-position. (The Zeeman frequency, ν_D, is close to 2.2 MHz). Using eq 3 and neglecting deuterium quadrupolar splittings, which are usually less than 0.1 MHz, deuterium hyperfine tensor principal values A_{11}, A_{22}, and A_{33} of 0.6, 1.6, and 2.6 MHz are estimated. The corresponding values for protons should be approximately 6.5 times larger (4, 11, and 17 MHz). The insert in Figure 4A shows the spectral range where the low-frequency ENDOR lines of the two larger hf-tensor principal values A_{22} and A_{33} of the α-proton are expected. Four weak features between 5 and 8 MHz are indeed present in the insert with corresponding hyperfine couplings between 17.7 and 12.9 MHz (0.63 and 0.46 mT). These lines are not observed in the spectrum of $W_a^\bullet$-d_5 (Figure 4B). We assign these lines to the two larger hf tensor principal

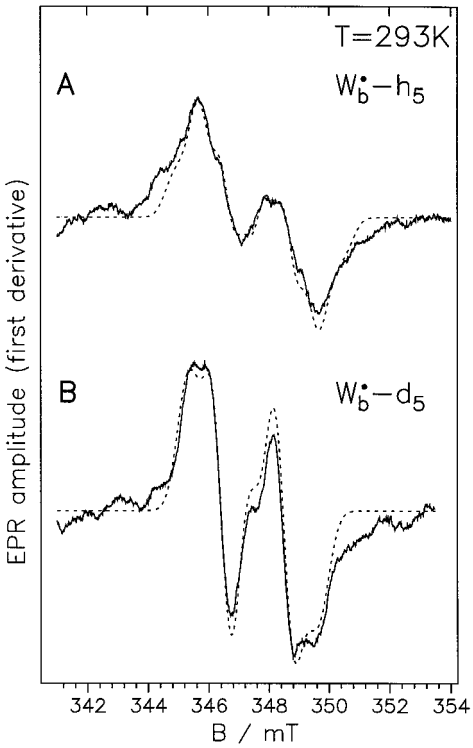

Figure 5. EPR spectra of the tryptophan radical $W_b^{\bullet}$ obtained with the stopped-flow accessory after mixing of aerobic *E. coli* apoprotein R2 Y122F (100 μM) and anaerobic ferrous iron (400 μM) at room temperature. Solid lines: experiment, dotted lines: best simulation (fit). (A) R2 with protonated tryptophan. (B) R2 with tryptophan-d_5. Experimental conditions: microwave power, 40 mW; field modulation, 100 kHz; amplitude, ±0.5 mT; 32 scans recorded within the lifetime of the radical after mixing (between 1 and 12 min) have been accumulated and the background has been subtracted. For the simulations a Gaussian line width of 0.46 mT was used; the obtained **g** and hf tensors are given in Table 1.

values A_{22} and A_{33} of *two* α-protons. The smallest principal values, A_{11}, are assumed to contribute to the line near 11.5 MHz or to the low-frequency shoulder of the matrix line starting at 12.5 MHz. The obtained principal values of the hf-tensor components, which were also used for the simulation of the EPR spectrum (Figure 3A), are listed in Table 1. According to the EPR simulations the principal axis of A_{33} is oriented in the molecular $x-y$ plane, whereas that of A_{22} is perpendicular to the plane (i.e. $A_{22} = A_{zz}$, see Figure 2).

Hydrogen Bond Proton: The ^{1}H-ENDOR spectrum of $W_a^{\bullet}$-d_5 clearly shows three line pairs (a,a′, b,b′ and c,c′; Figure 4B, insert) with corresponding anisotropic proton hf couplings of 5.4, 3.3, and 2.2 MHz. These couplings of $W_a^{\bullet}$-d_5 in R2 Y122F in H_2O buffer should only arise from the proton in the γ-position to C3 (i.e. to the proton bound to carbon Cα) or from a proton hydrogen bonded to N1 (see Figure 2). Since our RHF-INDO/SP calculations (see below) on the neutral radicals W111$^{\bullet}$, W107$^{\bullet}$, and W48$^{\bullet}$ predict in all cases hyperfine couplings ≤1.1 MHz for the proton in the γ-position to C3, we assign these couplings to the hf-tensor principal values A_{11}, A_{22}, and A_{33} of a proton hydrogen bonded to N1 of the neutral radical $W_a^{\bullet}$.

3.2. EPR Spectra of the Tryptophan Radical $W_b^{\bullet}$ at Room Temperature. Figures 5A and 5B show EPR spectra of protein R2 Y122F containing protonated tryptophan and tryptophan-d_5, respectively, obtained at room temperature (298 K) with the stopped-flow accessory in the time interval 1−10 min after mixing the aerobic apoprotein with anaerobic Fe^{2+}. The spectra are very similar to those reported earlier.[17,18] We denote the corresponding radical $W_b^{\bullet}$ (‘“room temperature tryptophan radical” in ref 17). Although the spectra are recorded in liquid aqueous solution, they exhibit powder-type character, since the tryptophans are immobilized in the protein R2 and the rotational motion of the protein R2 (molecular weight 86 kDa) is too slow to average out completely the large hyperfine anisotropy of the hf tensors of ^{14}N and the α-protons.

The simulation and fit of the powder-type EPR spectrum of $W_b^{\bullet}$-d_5 (Figure 5B) clearly revealed the presence of a large ^{14}N hf tensor with an isotropic value similar to that of $W_a^{\bullet}$ and only one coupling of a β-methylene proton. For the simulation of protonated $W_b^{\bullet}$ (Figure 5A) all parameters obtained from the fit of spectrum 5B were kept constant. Only the additional values of the two α-proton hf tensors were free fit parameters. Due to the poor signal-to-noise ratio the values for the α-proton tensor components have large errors. The **g** and hyperfine tensor components obtained from the fits and simulations are listed in Table 1.

Table 2. Calculated π-Spin Densities for Tryptophan Radicals and Experimental π-Spin Densities of $W_a^{\bullet}$

molecular position[a]	HMMO ref 13[b]	RHF-INDO/SP this work[c]	DFT[d] this work[e]	DFT[d] ref 31[f,g]	DFT[d] ref 34[h]	expt[i]
			Neutral			
N1	0.30	0.479	0.23	0.31	0.23	0.20
C2	0.04	−0.182	−0.01	−0.13	−0.03	≤|0.05|
C3	0.39	0.443	0.41	0.60	0.48	0.52
C5	0.09	0.101	0.14	0.19	0.19	0.17
C6	0.03	0.026	0.00	−0.05	−0.02	≤|0.05|
C7	0.06	0.056	0.11	0.15	0.15	0.15
C8	0.08	0.074	0.04	0.01	0.06	≤|0.05|
			Cation			
N1	0.08	0.242	0.14	0.14	0.12	n.d[j]
C2	0.42	0.112	0.16	0.19	0.14	n.d.
C3	0.39	0.297	0.27	0.37	0.30	n.d.
C5	0.10	0.197	0.18	0.25	0.24	n.d.
C6	−0.04	−0.031	−0.02	−0.09	−0.04	n.d.
C7	0.09	0.113	0.12	0.19	0.17	n.d.
C8	−0.01	0.086	0.10	0.06	0.13	n.d.

[a] For molecular position see Figure 2. [b] Extended Hückel/MacLachlan (Huyett et al.[13]). [c] This work, RHF-INDO/SP method (Plato et al.[27]), see text. Standard geometry, planar molecular system; R = CH_3, see Figure 2. Calculations performed for the X-ray geometries of W111$^{\bullet}$ and W107$^{\bullet}$ and W48$^{\bullet}$ in R2 yielded similar spin densities. [d] Density Functional Theory (DFT). [e] Program DMol, see text, energy minimized geometry, R = H, see Figure 2. [f] Jensen et al.,[31] 3-methylindole. [g] In a recent study O'Malley and Ellson[40] have calculated isotropic hfc's from the DFT wave functions using the same functional (B3LYP) and basis set (6-31G*) as in ref 31. The obtained values [mT] for the neutral 3-methylindole radical were as follows: 0.41 for N1, for protons: 0.11 (position 2), 1.68 (CH_3, for a rotating methyl group), −0.42 (position 5), −0.34 (position 7) and −0.06 (position 8). This is in excellent agreement with our experimental values (Table 1). [h] Walden and Wheeler,[34] indole. [i] From experimental hyperfine tensors of the neutral radical $W_a^{\bullet}$ given in Table 1 (see text). $W_a^{\bullet}$ was assigned to the neutral radical (see text). Data for a tryptophan cation radical in cytochrom *c* peroxidase are given in ref 13.

3.3. Spin Density Calculations. For an assignment of the observed hf tensors to specific positions within the molecule and a distinction between the cationic and the neutral radical we performed theoretical spin density calculations using the RHF-INDO/SP and the DFT approach (see Materials and Methods). The results of our calculations together with other reported theoretical results[13,31,34,40] are presented in Table 2. Comparison with experimental data will be discussed below.

4. Discussion

4.1. Spin Density Distribution, Oxidation State, and Assignment of $W_a^{\bullet}$. Oxidized tryptophan radicals can

(40) O'Malley, P. J.; Ellson, D. A. *Chem. Phys. Lett.* In press.

exist—depending on the pH value—in the cationic or the neutral form (deprotonated at N1, see Figure 2) with a pK of 4.3.[41] Therefore, neutral radicals would be expected for physiological pH values; however, a special (charged) protein environment or interactions with a nearby metal ion can stabilize the cationic form. In fact, the tryptophan radicals observed so far in two enzymes—cytochrom *c* peroxidase[13] and photolyase[42] —have been assigned to the cationic form, and to our knowledge no example has so far been reported for a protein-linked neutral tryptophan radical. The experimental distinction between these two forms is not trivial, but requires a detailed experimental characterization of the spin density distribution.

4.1.1. Spin Densities Obtained from the Experiments. Position C3: The two largest proton hyperfine couplings of $W_a^\bullet$ are assigned to the protons β_1 and β_2 (see Figure 2) because they have rather small anisotropy and are present also in the EPR spectra of $W_a^\bullet$-d_5 (Figure 3). The isotropic hfc of a β-proton is related to the neighboring carbon spin density ρ^π_c by

$$A_{iso}(H_\beta) = \rho^\pi_c (B' + B'' \cos^2 \theta) \qquad (4)$$

where B' and B'' are empirical constants and θ is the dihedral angle between the α-carbon p_z axis and the projected $C_\beta H_\beta$ bond[35,43] (see Figure2A). From the ratio of the hfc's of protons β_1 and β_2 and using $B' = 0$, $B'' = 5$ mT, and $\theta_1 + \theta_2 = 120°$, a spin density at carbon C3 of ρ^π (C3) = 0.57 and angles $\theta_1 = 13°$ and $\theta_2 = 133°$ have been deduced by Sahlin et al.[18] (see Figure 2). Using the slightly different constant $B'' = 5.8$ mT suggested for tyrosyl radicals[44] a somewhat smaller spin density ρ^π (C3) = 0.52 is obtained from the hfc of the β-protons of Table 2. This experimental value is in fair agreement with calculated spin densities for the tryptophan neutral radical[13,31,34] (see below).

Position N1: From the simulation of the EPR spectrum of $W_a^\bullet$-d_5 (Figure 3B) the ^{14}N hf tensor was obtained. The axis for the largest hf-tensor principal value A_{zz} ($=A_{||}$) is colinear with the g_{zz} axis. A_{zz} is obtained with high accuracy as 1.05 ± 0.02 mT, whereas the values for A_{xx} and $A_{yy} \leq 0.1$ mT ($A_{xx} = A_{yy} = A_\perp$) are only upper limits (see Table 1). Assuming axial symmetry the nitrogen p_z spin density can be estimated from the anisotropic hf tensor $\mathbf{A}'$ ($A'_{||} = A_{||} - A_{iso} = 2B$; $A'_\perp = A_\perp - A_{iso} = -B$) using the anisotropic hyperfine coupling ($B = {}^1/_2 A'_{||}$) tabulated in ref 45. Using the value of $B = 47.8$ MHz (1.706 mT) for ^{14}N (ρ^π(N) = 1) and assuming 0 mT ≤ $A_\perp$ ≤ 0.1 mT and $A_{||} = 1.05$ mT an experimental spin density ρ^π(N1) between 0.20 and 0.18 is obtained.

Positions C2 and C5 to C8. The spin densities at carbon positions 2 and 5 to 8 can be obtained from the respective α-proton hf tensors. Using Q factors of −2.48 mT,[9] π-spin densities of 0.17 and 0.15 are obtained from the respective isotropic parts of the two hf tensors assigned to α-protons (Table 1). These hf tensors, which are only observed in fully protonated $W_a^\bullet$ -h_5 (Figure 3A), must arise from α-protons attached to carbon atoms 2 and 5 to 8, since a N−H proton also should be observed in selectively deuterated $W_a^\bullet$-d_5 in H_2O buffer (i.e. Figure 3B). An important experimental result is that only with two rhombic α-proton hf tensors is the correct multiplicity of the subsplitting of the four prominent lines obtained in the simulated EPR spectra of fully protonated $W_a^\bullet$-h_5 (Figure 3A). The axes of the largest principal components of the two α-proton hf tensors are both in the molecular plane of $W_a^\bullet$ ($x-y$ plane, see Figure 2) and are rotated against each other by approximately 90° (±20°). Since both the **g** tensors and the hf tensor of N1 were found to be axially symmetric (see Table 1), the orientations of the hf-tensor axes x and y in the molecular $x-y$ plane remain undetermined. The angle of 90 ± 20° between the axes of the largest principal values of the two α-protons may however be used for assignments. For an isolated C−H fragment the axis of the largest principal value of the hf tensor is perpendicular to the C−H bond direction and perpendicular to the carbon p_z axis (i.e. in the plane of the π-system[35]). Therefore, angles of 60° and 120° would be expected between these principal axes for positions 5 and 6, and for positions 5 and 7, respectively. Only for positions 5 and 2 or for 8 and 2 are angles of approximately 90° are expected (see Figure 2). The hf tensor axes orientations are, however, also influenced by spin densities of neighboring atoms, making an assignment more difficult. For the assignment of the hf tensors of the two α-protons it was therefore important to calculate hf tensors of the α-protons including the contributions of all spin densities in the molecule (see below). Spin densities which were not determined experimentally had to be obtained by theoretical means.

4.1.2. Calculation of Dipolar Hyperfine Tensors from the Spin Density Distribution and Assignment of the α-Protons. In order to assign the observed two α-proton hf tensors to specific positions we have calculated the dipolar hf tensor for the protons at positions 2, 5, and 7 by integrating over all p_z spin densities of the tryptophan radical using Slater orbitals according to McConnell and Strathdee.[46] The isotropic part of the tensor was obtained from the respective carbon π spin densities $\rho(C_\pi)$ using the McConnell relation for an α-proton: A [mT] = $Q\rho(C_\pi)$ with $Q = -2.48$ mT as given by Bender et al.[9] Thereby the large spin densities ρ(N1) = 0.20, ρ(C3) = 0.52, ρ(C5) = 0.17, and ρ (C7) = 0.15 were taken from the experiment. The assignment of C5 and C7 was based on the results of the density functional (DFT) calculations for the neutral radical (see below and Table 2). For positions 2, 6, and 8 only upper limits for the spin densities (≤0.05) were estimated from the experiments (see above). Therefore the theoretical spin densities from the DFT method (this work) were used, which were all ≤0.05 in agreement with the experiments (Table 2, column 4). The calculation of the dipolar hf tensors was an important test to see whether the set of hf tensors obtained from the EPR/ENDOR spectra and simulations is consistent with the dipolar hyperfine couplings calculated from the spin density distribution in the molecule. This procedure is similar to that used by Huyett et al.[13]

Table 3 shows the α-proton hf tensors calculated in this way for positions 2, 5, and 7 of the $W_a^\bullet$ radical. Since all calculations predict the largest spin density in the six-membered ring for position 5, we assigned the larger experimental α-proton tensor (Table 1) to this position. The relative magnitudes of the calculated three principal values (Table 3) agree well with the experimental data (Table 1), also the experimental finding that the largest and the smallest principal values of the tensor (A_{11} and A_{33}) are both in the molecular $x-y$ plane (Figure 2) is in good agreement with the calculated data.

Since the angle between the largest principal components A_{11} of the hf tensors of the two α-protons was determined as 90 ± 20° and the C−H bonds at C5 and C2 also form an angle of

(41) Jovanovic, S. V.; Steenken, S.; Simic, M. G. *J. Phys. Chem.* **1991**, *95*, 684−687.
(42) Kim, S.; Sancar, A.; Essenmacher, C.; Babcock, G. T. *Proc. Natl. Acad. Sci. U.S.A.* **1993**, *90*, 8023−8027.
(43) Stone, E. W.; Maki, A. H. *J. Chem. Phys.* **1962**, *37*, 1326−1333.
(44) Fasanella, E. L.; Gordy, W. *Proc. Natl. Acad. Sci. U.S.A.* **1969**, *62*, 299−304.
(45) Wertz, J. E.; Bolton, J. R. *Electron Spin Resonance, Elementary Theory and Practical Applications*, Chapman and Hall: New York, 1986.
(46) McConnell, H. M.; Strathdee, J. *Mol. Phys.***1959**, *2*, 129−138.

Table 3. Calculated α - and H-Bond Proton Hyperfine Tensor Principal Values and Direction Cosines of Principal Axes for the $W_a^{\bullet}$ [a]

		molecular position[b]			
		2[c]	5	7	H-bond[d]
principal values[e] [mT]	A_{11}	0.23	−0.61	−0.60	0.187
	A_{22}	−0.04	−0.16	−0.10	−0.105
	A_{33}	−0.11	−0.50	−0.42	−0.084
direction cosines[e]	I_{1x}	0.920	−0.984	−0.460	0.230
	I_{1y}	−0.392	−0.180	0.888	−0.973
	I_{1z}	0.0	0.0	0.0	0.0

[a] Calculated from p_z spin densities using Slater $2p_\pi$ orbitals according to McConnell and Strathdee.[46] The isotropic part was added using $Q\rho(C_\pi) = -2.48$ mT for an α-proton (see text). Spin densities at N1, C3, C5, and C7 were those from the experiment (0.20, 0.52, 0.17, and 0.15, respectively); those for the other positions were from the DFT calculations (this work, see Table 2, column 4). The principal values A_{ii} agree well with the experimental values given in Table 1. [b] For molecular positions see Figure 2. [c] This tensor has been used in the EPR simulation of Figure 3A; it does not lead to an observable additional splitting (see text). [d] Calculated for a proton placed at a distance of 1.75 **Å** from N1 along the intersection of bonds N1−C9 and N1−C2. [e] Direction cosines of the axis corresponding to the respective A_{11} values in the molecular axis system (see Figure 2). The principal axes corresponding to A_{33} is parallel to the z-axis for all tensors.

90°, the hf tensor of the second α-proton (Table 2) should, in principle, be assigned to the proton at C2 (see above). However, the calculated hf-tensor components for the α-proton at this position using an atomic p-spin density at C2 from DFT for the neutral radical of −0.03[34] or −0.01 (this work, see Table 2) are much smaller than the experimental values and —according to the simulations—do not lead to an observable splitting in the EPR spectra. Only for spin densities $|\rho^{\pi}(C2)| \geq 0.16$ were the calculated hf-tensor components of comparable magnitude with the experimental values. We consider such a large spin density at C2, which should according to the calculations be negative in the neutral radical, as unlikely. Significant negative atomic p-spin density at C2 in the neutral radical is predicted by the INDO calculations and by the DFT calculations of Jensen et al.[31] Our DFT calculations for the neutral radical as well as those from Walden and Wheeler[34] did not yield significant negative spin densities at C2 (see Table 2). Therefore we prefer to assign the hf tensor of the second α-proton to position 7 based on the good agreement between calculated and experimental hf tensor components (compare Tables 1 and 3). The angle between the in-plane principal axes of A_{11} of the calculated hf tensor for positions 5 and 7 is 73° which is in agreement with the value obtained from the EPR simulations (90 ± 20°). With this assignment we also obtained an excellent agreement between all our experimental spin densities and those of DFT calculations in this work and in ref 34 for the neutral radical. Calculated hyperfine coupling constants based on DFT calculations of the neutral radical by O'Malley et al.[40] agree well with our experimental data for $W_a^{\bullet}$ (Table 2, footnote *g*). The experimentally determined π-spin densities for $W_a^{\bullet}$, 0.52 (C3), 0.20 (N1), 0.17 (C5), and 0.15 (C7), are indicated in Figure 2.

4.1.3. Neutral versus Cation Radical. One major difference between the neutral and cation tryptophan radical is the absence or presence of the covalently bound NH proton among the hf interacting nuclei. Using the published values for an α-proton attached to a nitrogen in a π-radical ($A_{11} = -4.14$ mT, $A_{22} = -2.68$ mT, and $A_{33} = -0.93$ mT for $\rho^{\pi}(^{14}N) = 1$[13]), components of the anisotropic hf tensor up to −0.8 mT are expected for such a proton in $W_a^{\bullet}$ ($\rho(N1) = 0.20$). Such a large coupling is not consistent with the EPR simulation of $W_a^{\bullet}$-d_5 in H_2O buffer (Figure 3B) which yielded an upper limit of 0.2 mT for any coupling in addition to two α-proton couplings assigned to C5 and C7. This clearly shows that $W_a^{\bullet}$ in R2 is in the deprotonated neutral radical state. This assignment is supported by the experimental observation of a hf-tensor component of 17 MHz for the tryptophan cation radical in cytochrome *c* peroxidase.[13] For this radical a nitrogen π-spin density of 0.14 was reported, which is considerably smaller than the value 0.20 which we find for $W_a^{\bullet}$ in R2. An increased spin density at N1 in the neutral radical compared with the cation radical is found in the DFT calculations consistent with our assignment. Finally, the DFT calculations predict for the cation radical, in addition to the α-proton couplings in the six-membered ring, a large α-proton coupling resulting from the large positive spin density at C2 (Table 2). Such an additional coupling is absent in $W_a^{\bullet}$. The simulation of the EPR spectrum of $W_a^{\bullet}$ (Figure 3A) clearly shows that only two large α-proton hf tensors are present.

Proton Hydrogen-Bonded to N1. The ENDOR spectrum of $W_a^{\bullet}$-d_5 shows additional hyperfine splittings of a weakly coupled proton. According to our RHF-INDO/SP calculations an assignment to the proton at the C_α-carbon of tryptophan is unlikely (see section 3.1.2). Therefore we assign it to a proton which is hydrogen bonded to N1. The obtained hf tensor components are given in Table 1. It should be noted that this tensor is traceless but not axially symmetric. At first sight this seems to be in contradiction to the point dipole approximation. In this model the hyperfine coupling is given by:

$$A^{H}(\Theta) = \frac{79}{r^3}\rho(3\cos^2\Theta - 1) \qquad (5)$$

where A is the coupling in MHz (2.802 MHz corresponds to 0.1 mT), ρ is the spin density at distance r (in Å) from the proton, and θ is the angle between the magnetic field and the vector connecting the electron and the proton.[47] For $\theta = 0°$ and 90° the principal values $A_{||}$ and $A_{\perp}$ are obtained, respectively. In the general case with a spin distribution over several atoms, however, a rhombic tensor is obtained. In $W_a^{\bullet}$ the hydrogen bonded proton is dipolar coupled to the spin density at N1 and also to the more remote but larger spin density at C3 (see Table 3 and Figure 2). The calculated dipolar hf tensor for this proton using the spin densities given in Table 3 and the McConnell−Strathdee procedure described above is in good agreement with the ENDOR data when the proton is placed 1.75 Å from N1 along the bisector of bonds N1−C2 and N1−C9. This suggests a fairly strong hydrogen bond to N1. Since the X-ray structure[4] shows that the carboxylate group of E204 is within the hydrogen bond distance to N1 of W111, we propose E204 as a hydrogen bond donor.

The missing strong coupling of a N−H proton, in spite of the large nitrogen spin density (0.2), and the weakly coupled proton in $W_a^{\bullet}$-d_5, the hf-tensor components of which are in excellent agreement with those calculated for a proton hydrogen bonded to N1, are both strong indications that $W_a^{\bullet}$ is in the neutral deprotonated form.

4.1.4. Spin Density Calculations/Assignments. π-spin densities for the oxidized tryptophan neutral and cation free radicals obtained from Hueckel molecular orbital calculations and atomic p-spin densities from DFT calculations published recently[13,31,34] are shown in Table 2. Results from RHF-INDO/SP and DFT calculations performed in our laboratory are also included. In all calculations at least 70% of the spin density in

(47) Feher, G.; Isaacson, R. A.; Okamura, M. Y.; Lubitz, W. In *Antennas and* Reaction Centers of Photosynthetic Bacteria, Structure Interaction, and *Dynamics*; Michel-Beyerle, M. E., Ed.; Springer: Berlin, 1985; pp 174−189.

the neutral radical is localized on N1 and C3, whereas there is almost zero or even negative spin density at C2. In the cation radical the spin density at N1 is strongly reduced compared with the neutral radical, and there is significant positive spin density (0.2 to 0.4) at C2. The calculated spin density distribution in the six-membered ring is similar for the neutral and cation radical. Depending on the theoretical method large spin densities (>0.06) in the six-membered ring in the neutral radical are obtained for positions 5 and 7 and—from HMMO and RHF-INDO/SP—also for position 8. The experimental spin densities of $W_a^\bullet$ agree very well with the results from the recently available density functional methods for the neutral radical, although there are slight differences between our results and those from refs 31 and 34, probably due to the different functionals and/or basis sets used (Table 2, columns 4 to 6). In a recent study O'Malley et al.[40] have calculated isotropic hfc's from the DFT wave functions using the same functional (B3LYP) and basis set (6-31G*) as in ref 31. The obtained theoretical isotropic hfc's for the 3-methylindole radical agree very well with the experimental data (see Table 2, footnote *g*). Recently, good agreement with DFT spin densities was also reported for the tryptophan cation radical in cytochrom *c* peroxidase.[13,31,34]

In addition to the RHF-INDO/SP calculations given in Table 2 we have also performed calculations for the neutral radicals of W48, W107, and W111 using the X-ray coordinates.[4] The X-ray structure[4] shows significantly different dihedral angles θ_1 and θ_2 for the β-methylene protons of these tryptophans in protein R2 (chain A): 119°, −121° for W48, 87°, −153° for W107, and −132°, −10° for W111 (compare Figure 2A). Based on the experimental hyperfine coupling constants (hfcs) and using eq 4 the dihedral angles of the β-protons were determined to be $\Theta_1 = 13°$ and $\Theta_2 = 133°$. $W_a^\bullet$ has previously been tentatively assigned in this way to W111$^\bullet$.[17,18] According to eq 4 the hfcs of these β-protons are also proportional to the π-spin density at carbon C3. The p_z-spin density distributions calculated with RHF-INDO/SP were very similar for these three tryptophan neutral radicals and were close to the values calculated for tryptophan neutral radicals with standard geometry (Table 2). The p_z-spin densities for C3 of W48$^\bullet$, W107$^\bullet$, and W111$^\bullet$ were 0.48, 0.49, and 0.46, respectively. The calculated isotropic hfc's of β_1 and β_2, obtained from the respective hydrogen s-spin densities, were 0.78 and 0.93 mT (W48), 0.03 and 1.97 mT (W107), and 1.1 and 2.2 mT (W111), accordingly. This is in agreement with an assignment of $W_a^\bullet$ to W111 and $W_b^\bullet$ to W107[18] and shows that only the different side chain geometry is responsible for the large differences in the hfc's of the two β-protons in these three tryptophans.

4.2. Spin Density Distribution, Oxidation State and Assignment of $W_b^\bullet$. The EPR spectra of $W_b^\bullet$ at room temperature (Figure 5) show pronounced anisotropies although they are recorded in liquid solution. This shows that $W_b^\bullet$ is immobilized and has a fixed orientation in the protein. The slow tumbling motion of the whole protein might however explain the smaller **g**- and ^{14}N hf-tensor anisotropy as compared with $W_a^\bullet$. The isotropic values for these tensors agree remarkable well for $W_a^\bullet$ and $W_b^\bullet$ (see Table 1). Based on the large ^{14}N hf-tensor components obtained from the fit of the EPR spectrum of $W_b^\bullet$-d_5 (Figure 5B) which are comparable with those of $W_a^\bullet$, we assign $W_b^\bullet$ observed at room temperature also to the neutral deprotonated radical state. The two α-proton hf tensors (Table 1) indicate a similar spin density distribution in the six-membered ring system as found for $W_a^\bullet$. The major difference between $W_b^\bullet$ and $W_a^\bullet$ is the presence of only *one* large β-proton hfc (1.6 mT) in the former radical. The hfc of the second β-proton is significantly smaller (≤0.2 mT) and not resolved in the EPR spectra (see Table 1 and Figure 5B). Based on the dihedral angles of the β-methylene protons of tryptophans W48, W107, and W111, given above, $W_b^\bullet$ was previously tentatively assigned to W107.[18] These assignments of $W_a^\bullet$ and $W_b^\bullet$ are compatible with the experimental finding that $W_b^\bullet$ is much weaker coupled to the diiron center than $W_a^\bullet$, since it can be observed by EPR at room temperature, whereas $W_a^\bullet$ is broadened beyond detection at elevated temperatures because of strong spin relaxation. This behavior was ascribed to the different distances of 4 and 8 Å between Fe2 and W111 ($W_a^\bullet$) and W107 ($W_b^\bullet$), respectively[17] (see also Figure 1).

4.3. Comparison with Tryptophan Radicals in Other Systems. Tryptophan radicals in irradiated single crystals of tryptophan HCl,[48,49] and tryptamine HCl[50] have been investigated by EPR and ENDOR. Thereby predominantly reduced species by H-addition to ring position C2 or C5 (see Figure 2) were observed for which two large β-proton hfc's of 3.6 and 4.2 mT[48,50] were determined. An oxidized tryptophan radical has also been reported in irradiated single crystals of tryptophan HCl[48] and was assigned to the neutral radical formed by abstraction of the N−H proton. For this radical a hyperfine splitting from one of the two β-methylene protons of 1.55 mT and from one α-proton of 0.7 mT was reported. Both values are consistent with a spin density distribution similar to that of $W_a^\bullet$ in R2 (see Figure 2). The ^{14}N hf tensor, however, was not determined.

Protein-linked tryptophan radicals have been identified by EPR and ENDOR so far only in cytochrome *c* peroxidase (CCP)[12,13] and DNA photolyase.[42] Using ENDOR spectroscopy at 4 K, specific deuteration, and site-directed mutagenesis, tryptophan W191 was identified as the radical site in CCP.[12] In a recent elaborate ENDOR study including selective ^{2}H-, ^{13}C-, and ^{15}N-labeling the hyperfine structure of W191$^\bullet$ in CCP has been elucidated, and this species has been identified as a protonated tryptophan cation radical.[13] In particular a large hyperfine coupling from an exchangeable proton was observed with ENDOR and assigned to the proton covalently bound to N1. The spin densities at positions N1, C2, C3, and C6 were determined to be 0.14, 0.35, 0.41, and −0.07, respectively. These values are in good general agreement with predicted values from DFT calculations for the cation radical of 3-methylindole in refs 31 and 34 and by our DMol calculations (see Table 2). In DNA-photolyase a spin-polarized tryptophan radical at W306$^\bullet$ has been observed by time-resolved EPR after photoexcitation at room temperature using selective ^{2}H- and ^{15}N-labeling and site-directed mutagenesis.[42] Based on the absence of a large ^{14}N hf coupling, W306 in DNA photolyase has also been assigned to a tryptophan cation radical. The two tryptophan radicals investigated in this study, $W_a^\bullet$ and $W_b^\bullet$ in R2 Y122F of *Escherichia coli* ribonucleotide reductase, represent the first examples of protein-linked oxidized neutral tryptophan radicals.

5. Concluding Remarks

The present study shows that neutral tryptophan radicals are generated in the vicinity of the diiron center in R2 Y122F at W111 and W107 under conditions that in the wild-type enzyme would generate the catalytically essential stable tyrosyl radical Y122$^\bullet$. A physiological role of these oxidized neutral tryptophan radicals is still open; so far they have only been observed in mutant R2 Y122F where the naturally occurring tyrosyl radical

(48) Flossmann, W.; Westhof, E. *Radiat. Res.* **1978**, *73*, 75−85.
(49) Sagstuen, E.; Byrkjeland, H. G.; Henriksen, T. *Radiat. Res.* **1978**, *74*, 10−22.
(50) Theisen, H.; Sagstuen, E. *J. Chem. Phys.* **1983**, *78*, 2254−2261.

$Y122^{\bullet}$ is absent. Residues W111 and W107 are not conserved in the R2 family. However, it was proposed that the conserved W48 is involved in long range electron transfer reactions both between R2 and R1[10] during catalysis and between solvent reductants and the metallocenter of R2 during the iron-reconstitution reaction.[18,54] Possibly, radicals are formed during the iron reconstitution of R2 Y122F at all three tryptophan positions with equal probability, but only the long-lived radicals $W111^{\bullet}$ and $W107^{\bullet}$ are observed after some 10 s, whereas the radical at W48 might be rapidly quenched due to its position near the surface of R2. Protein-linked oxidized neutral tyrosyl free radicals are well characterized and play an important role in electron-transfer processes in radical enzymes and in plant photosystem II.[7,51,52] Besides the functionally essential cationic tryptophan radicals found in cytochrome c peroxidase[13] and in DNA photolyase,[42] we have now demonstrated that oxidized neutral tryptophan radicals also can be involved in protein-mediated electron transfer processes.

Acknowledgment. The authors thank Prof. B. Hoffman (Northwestern University, Evanston) for helpful discussions concerning the dipolar hyperfine couplings and for making available the manuscript of the tryptophan cation radical in cytochrome *c* peroxidase prior to publication. Dr. G. Jensen (The Scripps Research Institute, La Jolla, CA) and Dr. O'Malley (University of Manchester, UK) are acknowledged for providing results of their density functional calculations on tryptophan radicals prior to publication. Dr. M. Plato (Freie Universität, Berlin) provided the RHF-INDO/SP and McConnell-Strathdee program. Financial support by the Deutsche Forschungsgemeinschaft (DFG; La 751/1−2 to G.L., F.M., and S.P.), Fonds der Chemischen Industrie to W. L., a German government fund (WIP; to G.L.), the Swedish Cancer Society, the Swedish Research Council for Engineering Sciences, the Swedish National Board for Technical Development (to B.-M.S.), the Swedish Natural Science Research Council, and the Bank of Sweden Tercentenary Foundation (to A.G.) are gratefully acknowledged.

JA960917R

(51) (a) Hoganson, C. W.; Babcock, G. T. *Biochemistry* **1992**, *31*, 11874−11880. (b) Hoganson, C. W.; Sahlin, M.; Sjöberg, B.-M.; Babcock, G. T *J. Am. Chem. Soc.* **1996**, *118*, 4672−4679.

(52) Stubbe, J. *Adv. Enzymol.* **1990**, *63*, 349−419.

(53) Stesmans, A.; Van Gorp, G. *Rev. Sci. Instrum.* **1989**, *60*, 2949−2952.

(54) Coves, J.; Delon, B.; Climent, I.; Sjöberg, B.-M.; Fontecave, M. *Eur. J. Biochem.* **1995,** *233*, 357−363.